The regulation of polar flagella assembly in *Pseudomonas putida*

Marta Pulido-Sánchez[a,b], Antonio Leal-Morales[a,b], Aroa López-Sánchez[a,b], Felipe Cava[c] and Fernando Govantes[a,b]#

Running title: Regulation of flagellar assembly

[a]Centro Andaluz de Biología del Desarrollo, Universidad Pablo de Olavide/Consejo Superior de Investigaciones Científicas/Junta de Andalucía. 41013 Sevilla, Spain

[b]Departamento de Biología Molecular e Ingeniería Bioquímica, Universidad Pablo de Olavide. 41013 Sevilla, Spain.

[c]The Laboratory for Molecular Infection Medicine Sweden (MIMS), Umeå Center for Microbial Research (UCMR), Science for Life Laboratory (SciLifeLab), Department of Molecular Biology, Umeå University, Umeå, Sweden.

Address correspondence to Fernando Govantes, fgovrom@upo.es

2-part abstract word count: 348 (249 + 99)

Manuscript word count: 8717

ABSTRACT

The Gram-negative bacterium *Pseudomonas putida* bears a tuft of flagella at a single cell pole. Here we use confocal microscopy imaging and quantitative image analysis to thoroughly characterize flagellar assembly in *P. putida*. In the timespan of a cell cycle, fluorescently labeled flagellar proteins are sequentially recruited to the new cell pole, starting with the MS-ring protein FliF and ending with the incorporation of the flagellin FliC concomitant to the following cell division. Assembly is highly efficient and cell pole-specific, accounting for >90% cells bearing polar flagella. Two polar landmark proteins, FlhF and FimV, are stably recruited to the new cell pole before the onset of flagellar assembly. FimV is required for permanent association of FlhF with the cell poles and regulates the timing of assembly by preventing early polar recruitment of the flagellar structural proteins. FlhF provides pole-selectivity to flagellar location by restricting FliF location to the cell poles and supporting highly efficient polar flagella assembly. In the absence of FlhF, flagellar assembly occurs at random locations and with very low efficiency, with most cells bearing foci of early flagellar proteins but only few displaying 1-2 short filaments. Finally, we show that poor FlhF-independent flagellar assembly results in faulty fT3SS function that limits secretion of the anti-FliA anti-σ factor FlgM, eventually leading to low expression of the Class III (FliA-dependent) flagellar genes. Our results shed new light on the mechanisms that ensure the timely assembly of the flagellar apparatus at the correct location in polarly flagellated bacteria.

IMPORTANCE

Bacterial flagella are complex rotating machines containing more than 30 different proteins. Bacteria bearing flagella at a single pole face a singular challenge: one daughter cell inherits all preexisting flagella and the other inherits none. To prevent this, a complete set of new flagella must be assembled at the non-flagellated pole in every cell cycle. Here we introduce FimV and FlhF, two polar landmark proteins whose coordinated action enables

the soil bacterium *Pseudomonas putida* to assemble a tuft of flagella at the correct polar location to ensure that both newborn cells inherit a complete set after cell division.

INTRODUCTION

For many bacteria, the planktonic stage is hallmarked by the synthesis of one or more flagella, intricate molecular engines that enable motility in a liquid or semi-solid medium by engaging in propeller-like rotation (Altegoer *et al.,* 2014). Flagella are made of three functional units: the basal body, a rotary machine embedded in the cell envelope; the filament, a long and thin helical structure that protrudes from the cells and acts as a propeller; and the hook, a rigid, curved element that connects basal body and filament. The basal body is in turn made out of five structural elements: the membrane-bound MS-ring lends support to the rest of components; the cytoplasmic C-ring modulates the direction of flagellar rotation; the flagellar type III secretion system (fT3SS) exports the extracellular flagellar components; the rod is a hollow cylinder that acts as a drive shaft for rotation and connects the MS-ring and the hook; and the cell wall-bound LP-ring surrounds the rod and plays the role of bushing. The flagellar stator, a membrane-bound complex that couples proton transport to the generation of torque is associated to the periphery of the basal body (Chevance & Hughes, 2008; Terashima *et al.*, 2008) **(Fig. 1)**. Flagellar function is modulated by the chemotaxis complexes, containing specific chemoreceptors and signal transduction proteins that interact with the C-ring to promote directional motion in response to concentration gradients (Matilla & Krell, 2017). The flagellar apparatus is sequentially assembled from the inside out (Chevance & Hughes, 2008), and flagellar genes are regulated by transcriptional cascades whose logic mirrors this assembly hierarchy (Smith & Hoover, 2009). Exquisite regulation of this process is paramount, as the synthesis and operation cost of the flagellar/chemotaxis system represents a substantial fraction of the energy resources of the cell (Macnab, 1996; Martínez-García *et al.*, 2014).

Bacterial flagellation patterns are diverse and genetically determined in a species-specific fashion. Peritrichous flagella are located around the bacterial cell. Polar flagella may occur as single units in one (monotrichous) or both poles (amphitrichous), or as tufts

containing a variable number of flagella (lophotrichous) in one or both poles. Less commonly, some bacterial species naturally bear their flagella in lateral or subpolar positions (Leifson, 1951; Schuhmacher *et al*., 2015). In peritrichously flagellated bacteria such as *Escherichia coli*, cell division results in a more or less even distribution of the existing flagella between both daughter cells to allow effective motility (Schuhmacher *et al*., 2015). In contrast, in bacteria displaying unipolar flagellation patterns only one of the daughter cells inherits the preexisting flagellar machinery after cell division, and a new set of flagella must be assembled at the opposite pole to support motility of the other daughter cell (Amako & Umeda, 1982). To this end, cells must deploy specific regulatory mechanisms to ensure the correct location and number of flagella and precise timing to match the emergence of the new functional flagella with the completion of cell division. Much like chromosome replication and segregation, the synthesis and assembly of unipolar flagella can be envisioned as a discontinuous process that must be initiated in each cell cycle and terminated concomitantly to cell division.

Pseudomonas putida is a well-characterized Gram-negative soil bacterium endowed with great metabolic versatility and a model organism for biodegradation of organic toxicants and bioremediation (Martins dos Santos *et al.*, 2004). During planktonic growth, *P. putida* displays unipolar lophotrichous flagellation. Most flagellar and core chemotaxis genes are located in a single chromosomal region, known as the flagellar cluster. Our recent work has unveiled the transcriptional organization of the flagellar cluster and the regulation of the flagellar genes by a three-tiered regulatory cascade (Leal-Morales *et al.*, 2022). FleQ is the master regulator of the flagellar/chemotaxis system in *P. putida*. FleQ activates σ^{54}-dependent Class II flagellar promoters to drive the synthesis of all the structural components of the basal body and the hook, and part of the core chemotaxis apparatus. FleQ also activates the synthesis of the alternative σ factor FliA. FliA is directly accountable for the activation of all the remaining (Class III) flagellar genes, encoding filament, stator and core

chemotaxis components (Leal-Morales *et al*., 2022), and multiple chemoreceptor-encoding genes (Rodríguez-Herva *et al.*, 2010; Marta Pulido-Sánchez, unpublished results).

The *P. putida* flagellar cluster encodes at least two proteins potentially involved in the spatial and numerical regulation of flagellar synthesis. The MinD-like ATPase FleN (also known as FlhG or YlxH), and the SRP family GTPase FlhF are major players in determining the location and number of flagella in numerous bacterial species. FlhF is generally considered a landmark protein that determines the location of the flagella, while FleN is a negative regulator that limits the number of flagella (reviewed by Kazmierczak & Hendrixson, 2013; Altegoer *et al.*, 2014; Schuhmacher *et al.*, 2015). Our recent work has shown that deletion of *flhF* in *P. putida* results in the assembly of only one or two flagella per cell at random positions (Navarrete *et al*., 2019).

P. putida genomes also encode orthologs of FimV, a *Pseudomonas aeruginosa* polar landmark protein. *P. aeruginosa* FimV promotes polar assembly of type IV pili (Carter *et al*., 2017), contributes to the activation of virulence genes *via* cAMP-mediated signaling (Inclan *et al*., 2016) and regulates the planktonic to biofilm transition (Bense *et al*., 2019; Schniederberend *et al*., 2019; Nicastro *et al*., 2020). FimV-related proteins, designated FimV, HubP or TspA, are present in multiple species of β- and γ-proteobacteria (Buensuceso *et al*., 2016). Members of the FimV/HubP/TspA family share a conserved architecture consisting of a N-terminal periplasmic domain, a single transmembrane region and a C-terminal cytoplasmic domain, but sequence conservation is limited to a periplasmic peptidoglycan-binding LysM motif (IPR018392) and a ~50 residue distal C-terminal motif (IPR020011) (Wehbi *et al*., 2011; Buensuceso *et al*., 2017). HubP proteins from *Vibrio and Shewanella* spp. are involved in flagellar and chemotaxis complex biogenesis and replication origin segregation among others (Yamaichi *et al*., 2012; Rossmann *et al*., 2015 Takekawa *et al*., 2016; Arroyo-Pérez & Ringgaard, 2021; Altinoglu *et al*., 2022; Rick *et al*., 2022).

Here we demonstrate the involvement of FlhF and FimV in the temporal and numerical regulation of flagellar biogenesis in *P. putida*. Our results suggest that the recruitment of FimV and FlhF to the new pole ensure the timely assembly of the flagellar apparatus at the appropriate polar location. These findings shed light on the complex regulatory mechanisms required to ensure the faithful inheritance of the motile phenotype by both daughter cells in unipolarly flagellated bacteria.

RESULTS

The temporal sequence of polar flagella assembly in *P. putida*

In order to characterize flagella assembly in *P. putida* we engineered fluorescent flagellar protein derivatives to use them as assembly reporters in confocal microscopy imaging experiments. To this end, we constructed fusions of FliF, the structural unit of the MS-ring and FliM, one of the three C-ring proteins, to GFPmut3. We also constructed a derivative of the main flagellin FliC bearing a serine-to-cysteine substitution at position 267 ($FliC^{S267C}$), to enable binding of maleimide-derived fluorochromes. All three proteins were produced in mini-Tn*7* derivatives from their natural promoters (P*fliE*, P*fliL* and P*fliC*) and translational start signals and were shown to complement the null swimming phenotypes of their cognate deletion mutants **(Fig. S1A)**. Polar FliF-GFP, FliM-GFP foci and tufts of $FliC^{S267C}$ filaments were readily observed in the wild-type *P. putida* strain KT2442 (a spontaneous rifampicin-resistant mutant of the reference strain KT2440) **(Fig. 2A)**, consistent with the polar location of the flagellar apparatus.

Although the flagellar apparatus is recognized to be sequentially assembled from the inside out (Chevance & Hughes, 2008), there is no consensus on the order in which the EBB (early basal body) components, namely the MS-ring, the C-ring and the fT3SS export gate, are added to the nascent structure (Kubori *et al*., 1997; Boll & Hendrixson, 2013, Morimoto *et al*, 2014; Li and Sourjik, 2011). To clarify this point, we assessed the ability of FliF-GFP and FliM-GFP to form fluorescent polar foci in *P. putida* KT2442 derivatives MRB194 and MRB175, bearing in-frame deletions of *fliF* and *fliM*, respectively, and MRB62 (henceforth designated "the $fT3SS^-$ mutant"), in which a miniTn*5*-Km insertion disrupts *fliP* and abolishes *fliQ*, *fliR* and *flhB* transcription, all encoding components of the fT3SS export gate **(Fig S2A)**. The polar distribution of FliF-GFP was unaltered in Δ*fliM* or $fT3SS^-$ cells. In contrast, FliM-GFP was predominantly distributed in the cytoplasm in the Δ*fliF* and $fT3SS^-$ mutants. Polar FliM-GFP foci were still present in a fraction of $fT3SS^-$ cells, but were absent in Δ*fliF* cells

(**Fig S2B)**. These results indicate that FliF, the structural component of the MS-ring, is recruited to the nascent flagellar location at the cell pole independently of the fT3SS or C-ring. In contrast, incorporation of FliM is strictly dependent on FliF and facilitated or stabilized by the fT3SS.

Next, we performed a set of quantitative analyses on the confocal microscopy images obtained from wild-type *P. putida* populations expressing the fluorescent flagellar proteins. Polar FliF-GFP and FliM-GFP foci and FliC^{S267C} filaments were observed in the vast majority of cells (92-93%) **(Fig. 2B)**. Conversely, very few cells (6-8%) displayed FliF-GFP or FliM-GFP foci in ectopic, non-polar locations, while ectopic FliC^{S267C} filaments were all but undetectable **(Fig. 2C)**. Selective flagellation at the cell pole is therefore a robust and stable phenotype that is preserved in a large part of the *P. putida* population. We also observed that polar flagella assembly is highly efficient, as shown by the nearly identical percentage of cells bearing the first (FliF) and last (FliC) assembled structural flagellar protein at their cell poles (93 and 92%, respectively).

To establish the order of the assembly of the flagellar proteins, we reasoned that newly divided *P. putida* cells only carry flagellar proteins at the old pole. Such unipolar distribution changes to bipolar during the cell cycle, as flagellar proteins are sequentially recruited and permanently bound to the nascent flagella at the new pole. Accordingly, the frequency of cells of a growing population showing bipolar distribution for each flagellar protein is expected to recapitulate their order of assembly (i.e., the sooner a protein is recruited to the new pole after cell division, the higher its bipolar distribution frequency). To test this hypothesis, we assessed the cellular distribution of the fluorescent flagellar proteins in wild-type *P. putida* **(Fig. 2B)**. The frequency of bipolarly distributed foci or filaments was 48%, 28% and 2% for FliF-GFP, FliM-GFP and FliC^{S267C}, in full agreement with the expected MS-ring>C-ring>filament assembly hierarchy **(Fig. 2B)**.

In a growing bacterial population, cells become longer over time between cell divisions. Hence, there is a direct correlation between cell age (i.e., time elapsed from the previous cell division) and length (Vischer *et al*., 2015). To establish the relationship between individual flagellar protein recruitment and cell age, we assessed the frequency of bipolar distribution in relation to cell length from fluorescence demographic maps of length-sorted images of wild-type cells expressing FliF-GFP, FliM-GFP or FliC^{S267C} **(Fig. S3)**. The bipolar distribution frequency *vs.* cell length plots derived from this analysis showed that the frequency of bipolar distribution increases with cell length for all four proteins **(Fig. 2D)**. In addition, an inverse correlation was observed between bipolar distribution frequency **(Fig. 2B)** and the cell length range at which each protein accumulated at the new pole **(Fig. 2D)**, with FliF-GFP being recruited at the shortest cell length range (50% bipolar distribution at ~3.3 μm), followed by FliM-GFP (50% bipolar distribution at ~4.2 μm). The maximum bipolar distribution frequency of FliC^{S267C} (~40%) only occurred at the longest cell range (>5 μm), highlighting the notion that filaments emerge as cells approach cell division **(Fig. 2D)**. Taken together, these results are consistent with the stable recruitment of the flagellar proteins to the new cell pole in the time elapsed between cell divisions according to the sequence FliF>FliM>FliC.

FimV and FlhF are required for full flagellar function in *P. putida*

The *P. putida* KT2440 ORF PP_1993 encodes an ortholog of *P. aeruginosa* FimV. *P. putida* FimV displays 55% identity and 68% similarity to its *P. aeruginosa* counterpart. To assess the possible involvement of FimV in flagellar assembly we constructed MRB97, a derivative of *P. putida* KT2442 bearing a complete deletion of PP_1993. KT2442-derived Δ*flhF* and Δ*fleQ* mutants MRB69 and MRB52 were previously described (Navarrete *et al*., 2019). The Δ*fimV* and Δ*flhF* mutants displayed 39% and 55% reduction in motility halo diameter relative to the wild-type in a soft agar-based swimming assay **(Fig. S1B and C)**. The non-motile Δ*fleQ* mutant, used here as negative control, did not spread from the

inoculation point. These results indicate that FimV and FlhF are not essential to flagellar motility, but are required for full flagellar function.

FimV and FlhF are targeted to the new cell pole prior to the onset of flagellar assembly

The cellular location of FlhF was assessed by expressing a fluorescent C-terminal FlhF-GFP fusion from its physiological P*flhF* promoter and translational start signals. We previously noted that *fimV* transcription is continuous with that of the upstream gene, *asd* (Marta Pulido, Sánchez, unpublished). Therefore, we also used a FimV-GFP fusion expressed from the promoter region upstream of *asd* (P*asd*), followed by the *fimV* translational initiation region to address the cellular location of FimV. Expression of the FlhF-GFP and FimV-GFP fusions fully complemented the swimming defects of the Δ*flhF* and Δ*fimV* mutants, confirming the presence of a promoter activity in the cloned P*asd* fragment **(Fig. S1B)**.

FimV-GFP and FlhF-GFP formed fluorescent foci at the cell poles in wild-type *P. putida* **(Fig. 3A)**. The distribution frequencies of both proteins were notably similar: 60% and 58% of the cells displayed bipolar FimV-GFP and FlhF-GFP foci, respectively, while unipolar distribution was observed in 33% and 34% of the cells, and cells lacking polar foci were rare (7%) **(Fig. 3B)**. The bipolar distribution frequencies were greater than those of the flagellar structural proteins, suggesting that FimV and FlhF recruitment to the new cell pole may occur at an earlier time. This was confirmed by the bipolar distribution frequency *vs.* cell length plots derived from the fluorescence demographic maps of FimV-GFP and FlhF-GFP **(Fig. 3C and Fig. S4A)**. The bipolar distribution frequencies of both fusion proteins increased with cell length, with 50% bipolar distribution already present in the shortest cells, and reached a plateau in cells above 3-3.5 μm corresponding to 80-90% cells. Interestingly, FimV and FlhF foci were observed at the midcell region in a small percentage of cells, but were substantially enriched (up to ~45%) in the longest, predivisional cells **(Fig. S2B)**, strongly suggesting that both proteins are recruited to cell division sites around the time of

cell division. Taken together, these results indicate that FimV and FlhF are located to the new cell pole early in the cell cycle and prior to the onset of flagellar assembly. The similarity of bipolar and midcell distribution frequency values obtained with FimV-GFP and FlhF-GFP precluded the establishment of a recruitment sequence for these two proteins **(Fig. 3B and C)**.

FimV regulates FlhF association with the cell poles

Because FimV and FlhF appear to accumulate at the new cell pole with similar dynamics **(Fig. 3B and C)**, we hypothesized that they may influence each other recruitment. To test this possibility, we evaluated the impact of *flhF* and *fimV* deletions on intracellular FimV-GFP and FlhF-GFP location, respectively. The polar distribution of FlhF-GFP was deeply disturbed in the absence of FimV, with less cells bearing polar FlhF-GFP foci and higher fluorescence intensity distributed in the cell cytoplasm **(Fig. 3A)**. Quantitative analyses of the microscopy images revealed that the frequency of cells not bearing polar FlhF-GFP foci was increased 6-fold (41% *vs.* 7% in the wild-type), and the polar distribution was shifted from 34% unipolar and 58% bipolar in the wild-type to 50 and 9%, respectively **(Fig. 3B)**. The bipolar distribution frequency *vs.* cell length plots derived from the demographic maps **(Fig. 3C)** showed that the frequency of bipolarly distributed FlhF-GFP was decreased to a maximum of ~30% in shorter cells, and diminished further with length to ~15% at the longest cell range indicating that, in the absence of FimV, FlhF fails to accumulate at the new pole during the cell cycle. Assessment of the fluorescence intensity of the polar foci also revealed a >2-fold decrease in median fluorescence relative to the wild-type, suggesting that less FlhF-GFP molecules are present at the foci found in the Δ*fimV* cells **(Fig. 3D)**. Decreased polar targeting was accompanied by a 5-fold increase in the frequency of cells bearing ectopic fluorescent foci at non-polar locations in the Δ*fimV* mutant, resulting in a 4-fold increase in the frequency of cells bearing three or more FlhF-GFP foci **(Fig. 3E and F)**. In contrast, the lack of FlhF did not significantly change the intracellular

location of FimV-GFP, which showed unaltered frequencies of bipolar and unipolar distribution, a similar accumulation dynamics relative to cell length, comparable foci intensity distribution, and similarly low frequency of ectopic foci relative to those observed in the wild-type **(Fig. 3A-F)**, suggesting that FlhF has no role in FimV polar recruitment.

To test the impact of FimV on FlhF location further, the dynamics of FlhF-GFP accumulation at the cell poles was monitored by time-lapse fluorescence microscopy **(Fig. 4 and Videos SV1 and SV2)**. In the wild-type, FlhF-GFP foci were observed at the new cell pole shortly after cell division and remained at all poles for the duration of the experiment (i.e., 300 minutes). Deletion of *fimV* did not prevent FlhF-GFP recruitment to the new poles, but newly formed foci were not stable in the absence of FimV and were eventually disassembled (median lifespan of 70 minutes) **(Fig. 4 and Fig. S5)**. These results suggest that FlhF is targeted to the new cell pole early in the cell cycle in a FimV-independent fashion, but FimV is required to stabilize the association of FlhF with the cell pole. On the other hand, such permanent sequestration may in turn prevent FlhF nucleation at non-polar locations.

FlhF and FimV regulate the recruitment of the flagellar proteins

To determine the possible influence of FlhF and FimV on the recruitment of individual flagellar proteins we evaluated the impact of *flhF* and *fimV* deletions on the cellular distribution of FliF-GFP, FliM-GFP and FliC^{S267C}. Notably, the location of the three proteins was no longer restricted to the cell poles in the Δ*flhF* mutant **(Fig. 5A)**. Instead, most cells displayed multiple randomly-located FliF foci (median=5 foci/cell), accounting for 71% cells with polar foci and 94% with ectopic foci **(Fig. 5A-D)**. In contrast, the FliM-GFP fusion was generally distributed in the cytoplasm, but most cells also displayed a small number of foci (median=2) at polar (46%) and/or non polar (75%) locations **(Fig. 5A-D)**. Strikingly, most Δ*flhF* cells lacked FliC^{S267C} filaments, with only 3% displaying polar filaments **(Fig. 5A and B)** and 12% ectopic filaments **(Fig. 5C)**. Filaments formed at both polar and ectopic positions

of the Δ*flhF* mutant cells were few (1 or 2 units in ~90% of the flagellated cells) **(Fig. 5E)**, short (often less than one wavelength), and not bundled in tufts **(Fig. 5A and Fig. S6)**. These observations suggest that FliF can nucleate at random locations of the cell membrane to promote further assembly of the flagellar apparatus, albeit with much reduced efficiency. Taken together, our results indicate that FlhF restricts the recruitment of flagellar proteins to the cell poles and is necessary for efficient flagellar assembly at this location.

Unlike the Δ*flhF* mutant, most Δ*fimV* cells displayed polar FliF-GFP or FliM-GFP foci and $FliC^{S267C}$ filaments. Visual examination did not detect any morphological differences between the polar flagella of the wild-type **(Fig. 2A)** and the Δ*fimV* mutant **(Fig. 5A)**. Quantitative analyses revealed that the overall frequencies of cells bearing polar foci or filaments was ~90% for all three proteins **(Fig. 5B)**, similar to those in the wild-type **(Fig. 2B)**. In addition, the distribution of the total number of filaments in both strains was also notably similar **(Fig. 5E)**. Despite these similarities, the Δ*fimV* mutant displayed two discrepant features in the distribution of the flagellar proteins relative to the wild-type. On the one hand, ectopic FliF-GFP and FliM-GFP foci were 5-fold more frequent in the Δ*fimV* mutant **(Fig. 5C)**. In addition, although ectopic $FliC^{S267C}$ filaments were only found in less than 1% of the cells, they were still 10-fold more frequent than in the wild-type strain. These results suggest that FimV prevents the accumulation of flagellar assembly intermediates at ectopic sites. On the other hand, the Δ*fimV* mutant displayed increased bipolar distribution frequency of FliF-GFP (86%), FliM-GFP (64%) and $FliC^{S267C}$ (10%) **(Fig. 5B)**, compared with 48%, 28% and 2%, respectively, observed in wild-type cells **(Fig. 2B)**. The bipolar distribution frequency *vs.* cell length plots derived from the demographic maps of length-sorted cells **(Fig. S7)** showed that flagellar proteins with increased bipolar distribution were targeted to the new pole at shorter cell lengths in the Δ*fimV* mutant background **(Fig. 5F)**. In addition, both FlhF and FliF accumulated at midcell with 4-fold increased frequency, and midcell foci were further enriched in long, predivisional cells, suggesting that deletion of *fimV*

causes the onset of flagellar assembly to overlap with cell division (**Fig. S8)**. These results indicate that FimV regulates the timing of flagellar assembly by preventing early recruitment of the flagellar proteins.

FlhF is required for fT3SS activity and full Class III flagellar gene expression

The results above reveal that, while FliF-GFP and FliM-GFP foci are present in a large percentage of Δ*flhF* cells, FliC^{S267C} filaments are conspicuously absent in most. Since rod, hook and filament components (but not those of the MS- and C-rings) are secreted by way of the fT3SS, we considered the possibility that flagellar secretion may be impaired in the absence of FlhF. In *E. coli* and other bacteria, the anti-σ factor FlgM is secreted to the medium *via* the fT3SS to release inhibition of its cognate σ factor FliA (Chevance & Hughes, 2008, Smith & Hoover, 2009). To show if this regulatory mechanism is conserved in *P. putida*, we used plasmid-borne transcriptional fusions of the flagellar promoters P*flhA* (Class II) and P*cheA* (Class III) to a dual *gfp-lacZ* reporter (Leal-Morales *et al*., 2022) and assessed their expression by means of β-galactosidase assays in Δ*fleQ*, Δ*fliA*, Δ*flgM* and Δ*fliA*Δ*flgM* strains **(Fig. S9)**. P*flhA* expression was abolished in the absence of FleQ, but remained unaltered in the Δ*fliA*, Δ*flgM* or Δ*fliA*Δ*flgM* strains, consistent with its classification as a Class II promoter (Leal-Morales *et al*., 2022). P*cheA* expression was severely decreased in the absence of FleQ or FliA (Leal-Morales *et al*., 2022), but was increased 5-fold in the Δ*flgM* mutant, indicating that FlgM is a negative regulator of P*cheA* transcription. The β-galactosidase levels obtained in the absence of both FliA and FlgM were low and similar to those in the Δ*fliA* mutant, indicating that FlgM-mediated repression is dependent on the presence of FliA. This is fully consistent with a role of FlgM as a FliA-specific anti-σ factor FlgM in *P. putida*. Next, we sought to evaluate FlgM secretion as a possible reporter for fT3SS function. To this end, we produced C-terminally FLAG-tagged FlgM from the salicylate-inducible P*sal* promoter in a mini-Tn7 derivative and detected it in wild-type and fT3SS^{-} cell fractions and culture supernatants by Western blot using an anti-FLAG antibody

(**Fig. 6A**). A band compatible with the molecular weight of FlgM-FLAG (~12 kDa) was detected in both cell fractions and in the wild-type strain supernatant, but was absent in that of the fT3SS$^-$ mutant, indicating that FlgM is secreted by way of the flagella in *P. putida*. The same assay performed in the Δ*flhF* mutant yielded a similar FlgM-FLAG band in the cell fraction, but not in the supernatant, indicating that FlhF is required for fT3SS-dependent FlgM secretion.

A simple prediction derived from the FlgM secretion defect in the Δ*flhF* mutant is that FlgM will persist to inactivate FliA, leading to downregulation of the Class III promoters in this background. To test this hypothesis, we assessed the effect of *flhF* deletion on the expression the Class III flagellar promoter P*cheA* using the aforementioned dual reporter fusion (Leal-Morales *et al*., 2022) (**Fig. 6B**). Expression measured as GFP fluorescence was high in the wild-type and greatly decreased in the Δ*fliA* strain, as shown above. FliA-dependent P*cheA* activation was all but abolished in the fT3SS$^-$ and *fliF* mutants, both of which are impaired in flagella-dependent secretion. Deletion of *flhF* also caused a 3-fold decrease in P*cheA* expression, consistent with the defect in FlgM secretion in this background shown above. A comparable reduction in fluorescence levels in the Δ*flhF* strain was also observed with two additional fusion constructs based on the Class III promoters P*fliC* and P*motA* (Leal-Morales *et al*., 2022) **(Fig. S10)**. Taken together, our findings suggest that the poor efficiency of flagellar assembly in the absence of FlhF prevents normal fT3SS function, leading in turn to faulty FlgM secretion and a generalized defect in Class III flagellar promoter activation by FliA.

DISCUSSION

Spatiotemporal control of flagellar assembly is a critical aspect of the regulation of motility in polarly flagellated bacteria (Kazmierczak & Hendrixson, 2013; Schuhmacher *et al*., 2015). Because of the asymmetry of their unipolar flagellation pattern, motile *P. putida* cells can only transmit their flagellar machinery to one of their offspring upon cell division. Hence, to secure motility of both daughter cells, *P. putida* must (i) identify the new pole as a site for *de novo* flagella assembly, (ii) assemble a tuft of flagella at this site, and (iii) coordinate the timing of such assembly with the cell cycle to ensure emergence of the new flagella around the time of the following cell division. This work uses a methodology based on quantitative analysis of confocal microscopy images of bacterial populations to (i) characterize polar flagellar assembly in *P. putida*; (ii) expand on the function of a previously described regulatory element, FlhF (Navarrete *et al*., 2019); and (iii) characterize the involvement of a novel regulatory element, the polar landmark protein FimV, in the spatiotemporal control of flagellar assembly in *P. putida*.

The assembly hierarchy of the flagellar EBB is controversial, as conflicting evidence suggest that the earliest assembled structure is either the MS-ring or the fT3SS export gate, which is located at the inner opening of the MS-ring **(**Kubori *et al*., 1997; Boll & Hendrixson, 2013; Morimoto *et al*, 2014**;** Li and Sourjik, 2011**)**. We show here that FliF location at the cell poles is independent of the presence of the fT3SS export gate in *P. putida* **(Fig. S2)**. We propose that FliF is the earliest flagellar component to be recruited to cell pole, although we favor the view polymerization of FliF into a functional MS-ring is likely simultaneous and coordinated with the assembly of the export gate, as previously suggested **(**Morimoto *et al.*, 2014**)**. We also show that polar location of FliM is dependent of the presence of FliF. FliM is a cytoplasmic protein with no membrane-binding domains, and its incorporation to the growing flagellar structure has been shown to require the previous assembly of the MS-ring

and the incorporation of FliG, a second C-ring protein that interacts with both FliF and FliM, in different bacteria (Macnab, 2003; Apel & Surette, 2008; Armitage & Berry 2020).

Wild-type *P. putida* permanently carries a tuft of flagella at a single pole. After cell division, a new pole is created and eventually targeted for *de novo* assembly of a flagellar apparatus intended to provide motility to the daughter cell that inherits that pole after the following cell division. Based on this, we made the following assumptions: (i) flagellar proteins are present only at the old pole after cell division and sequential incorporation of flagellar proteins to the new pole causes a shift of the distribution from unipolar to bipolar, (ii) in a randomly sampled growing bacterial population, the frequency of bipolar distribution of a flagellar protein correlates inversely with its time of recruitment to the new pole (i.e., proteins recruited early display higher frequency of bipolar distribution and those recruited later lower frequency), and (iii) because *de novo* flagellar assembly is circumscribed to the time elapsed between one cell division and the next and cells grow continuously during this period, early recruited proteins are more likely to display bipolar distribution in shorter cells than proteins recruited at later times, i.e., cell length serves as a proxy for time in this context (Vischer *et al*., 2015). Quantitative analysis of confocal microscopy images of cells bearing fluorescent derivatives of FliF, FliM and FliC revealed that the flagellated phenotype is very prevalent in wild-type *P. putida*, with >90% cells displaying flagella, and highly selective for the cell poles, with non-polar flagella being nearly undetectable. Flagellar assembly at the cell poles is highly efficient, with nearly identical percentages of cells bearing the first (FliF) and last (FliC) assembled protein at their cell poles. The bipolar distribution frequency was highest in FliF, intermediate in FliM, and very low in FliC, consistent with the expected FliF>FliM>FliC assembly sequence. These results were confirmed when bipolar distribution frequency was plotted against cell length. All three proteins increased their bipolar distribution frequency with cell length, suggesting that recruitment leads to stable association to the new pole. Using the length at which 50% cells displayed bipolar

association (BP_{50}) as a midpoint reference value, we determined that FliF and FliM had BP_{50} values of ~3.3 and ~4.2 µm, while FliC never achieved a 50% bipolar distribution. Notwithstanding the measurement errors associated to these calculations, it is reasonable to conclude that FliF is recruited preferentially during the first half of the cell cycle and FliM early in the second half, while FliC incorporation largely occurs in predivisional or dividing cells at the end of the cycle.

We have explored the possible function of the landmark proteins FlhF and FimV in polar flagella assembly in *P. putida*. Deletion mutants lacking FlhF or FimV are both motile and moderately defective in flagellar function as judged by their phenotypes in swimming assays **(Fig. S1)**. FlhF is a known determinant of flagellar location in multiple bacteria (Schuhmacher et al, 2015), including *P. putida* (Pandza *et al*., 2000; Navarrete *et al*., 2019). The highly similar *P. aeruginosa* FimV protein regulates twitching motility (Carter *et al*., 2017), cAMP-mediated signaling (Inclan *et al*., 2016) and planktonic-to-biofilm transition (Nicastro *et al*., 2020; Bense *et al*., 2019; Schniederberend *et al*., 2019), but is not involved in flagellar function (Buensuceso *et al*., 2017). FimV is part of the FimV/HubP/TspA family of polar landmark proteins. These proteins are highly variable in size and sequence but share a common architecture, with an N-terminal periplasmic domain featuring a peptidoglycan-binding LysM domain, followed by a transmembrane helix and a C-terminal cytoplasmic domain containing a variable number of tetratricopeptide repeat motifs (Buensuceso *et al*., 2016). However distantly related to FimV, HubP proteins have been shown to regulate flagellar assembly in *Vibrio cholerae*, *Shewanella putrefaciens*, *Vibrio alginolyticus*, *Vibrio vulnificus* and *Vibrio parahemolyticus* (Yamaichi *et al*., 2012**;** Rossmann *et al*., 2015; Takekawa *et al*., 2016; Park *et al*., 2019; Arroyo-Pérez & Ringgaard, 2021; Dornes *et al*., 2024). Our results highlight the fact that members of the FimV/HubP/TspA family adopt specific roles that are adapted to the particular physiological needs of their host organism.

FimV and FlhF are targeted to the cell division plane or the new poles during or shortly after cell division and remain permanently associated to the new poles **(Fig. 3A-C, Fig. 4, Fig. S4 and Video SV1)**. Recruitment of FimV to the midcell region is consistent with FimV-dependent recruitment of the type IVa pilus machinery to future cell division sites in *P. aeruginosa* (Carter *et al*., 2017) and the midcell localization of HubP in *V. cholerae* (Yamaichi *et al*., 2012) and *S. putrefaciens* (Rossmann *et al*., 2015), and may involve interaction of its periplasmic domain with septal peptidoglycan (Wehbi *et al*., 2011), or components of the cell division machinery (Galli *et al*., 2017). We have shown that FlhF can nucleate at both polar and non-polar locations in a FimV-independent fashion **(Fig. 3A and B)**, but its association to the cell poles is stabilized by FimV **(Fig. 3A and B, Fig. 4, Fig. S5 and Videos SV1 and SV2)**. While FlhF is intrinsically able of insertion in the cell membrane in *Vibrio* spp. (Kusumoto *et al*., 2008; Green *et al*., 2009), polar recruitment of FlhF in *P. putida* requires the participation of the membrane maintenance $TonB_m$-PocAB complex (Ainsaar *et al*., 2019), which is not polarly located itself. We propose that random FlhF insertion at the cell membrane is aided by $TonB_m$-PocAB, but FimV-mediated stabilization only occurs at the cell poles. There are no precedents of members of the FimV/HubP/TspA family regulating the stability of the polar association of FlhF in any organism.

We have examined in detail the function of FlhF in the regulation of polar flagellar location in *P. putida*. The analysis of microscope images of *P. putida* cells expressing fluorescently labelled FliC shows that most (>90%) wild-type cells bear one to >3 polar flagella. In contrast, most (~85%) Δ*flhF* cells are aflagellated, and those bearing flagella display only one or two units with unusually short filaments at random locations **(Fig. 5A, B and E and Fig. S6)**. Delocalization of polar flagella confirms that FlhF is indeed required for the cell pole specificity of flagellation in *P. putida* (Pandza *et al*., 2000; Navarrete *et al*., 2019). General inhibition of flagellation has been found in *flhF*-null mutants in other bacterial species (Green *et al*., 2009; Kusumoto *et al*., 2008). However, it was not previously detected

in *Pseudomonas* spp. (Pandza *et al*., 2000; Murray and Kazmierczak, 2006; Navarrete *et al*., 2019).

Fluorescent FliF and FliM did not reproduce the pattern shown above for FliC. Instead, most Δ*flhF* cells displayed randomly located FliF and FliM foci, although the number of foci was far greater in FliF (median = 5) than in FliM (median = 2) **(Fig. 5D)**. Because FliM is diffusely located at the cytoplasm in the absence of FliF **(Fig. S2B)**, it is apparent that FliF can recruit FliM to the cell surface in the absence of FlhF. The occurrence of FliF and FliM as discrete loci as opposed to their diffuse localization in the cell envelope suggest that most Δ*flhF* cells initiate flagellar assembly at polar and ectopic locations at least to the point of FliM nucleation at the cell membrane. The ability of the MS-ring to self-assemble and promote assembly of the C-ring has been previously described in *Salmonella* (Katayama *et al*., 1996; Kubori *et al*., 1997). We have not explored the extent of MS-ring and C-ring assembly in the absence of FlhF. However, because flagellar filaments are present in a small fraction of Δ*flhF* cells, it is evident that the absence of FlhF is not an insurmountable barrier to flagellar assembly. We conclude therefore that polar and non-polar flagellar assembly in the absence of FlhF is intrinsically inefficient, with a major bottleneck occurring after FliM nucleation and before FliC incorporation. Taken together, our results strongly suggest that FlhF acts primarily by luring FliF to assemble at the cell pole. Such recruitment serves a dual purpose: it directs specific and highly efficient assembly of the flagellar structure at the cell poles and prevents initiation of (for the most part) faulty flagellar assembly elsewhere.

We have explored the flagellar assembly defect of the Δ*flhF* mutant further by using the FliA-specific anti-σ factor FlgM as a secretion reporter. Our results indicate that secretion by way of the flagella is impaired in the Δ*flhF* mutant **(Fig. 6A)**. This defect is a likely consequence of unsuccessful assembly of the fT3SS and explains the absence of filament, an extracellular secreted structure, in most Δ*flhF* cells. We have demonstrated that the

fT3SS is essential to FlgM secretion and Class III gene activation, consistent with the use of FlgM secretion as an assembly checkpoint to enable late flagellar gene transcription (Chevance & Hughes, 2008, Smith & Hoover, 2009). Accordingly, an indirect effect of the inability of the Δ*flhF* mutant to evict FlgM from the cells is a reduction in Class III promoter expression **(Fig. 6B and Fig. S9)**, indicating that FlhF indirectly stimulates Class III transcription by enabling FlgM secretion. A negative effect of *flhF* deletion on late flagellar gene expression has been documented in *P. aeruginosa* (Murray & Kazmierczak, 2006), *V. cholerae* (Correa *et al*., 2005) *V. vulnificus* (Kim *et al*., 2012), *Campylobacter jejuni* (Ren *et al*., 2018; Li *et al*., 2022) abd *Helicobacter pylori* (Niehus *et al*., 2004), but the mechanisms behind this phenomenon have not been explored. It is worth noting that the shortage of flagellin units due to low expression from the P*fliC* promoter may suffice to explain the unusually short length of the filaments in the Δ*flhF* mutant (**Fig. 5A and Fig. S6)**.

Since FimV stabilizes the association of FlhF with the cell poles, we questioned whether the absence of FimV has any impact on any of the functions of FlhF. The Δ*fimV* mutant displayed polar tufts with similar flagellar numbers and morphology to the wild-type **(Fig. 5A and E)** along with non-polar FliF- and FliM-containing assemblies that rarely led to filament completion, as discussed above **(Fig. 5C-E)**, indicating that FimV-mediated stabilization of FlhF association with the cell pole is not required for the assembly of polar flagella, but is necessary to prevent abortive flagellar assembly at ectopic positions.

We have assigned a second, previously undescribed, role to FimV in determining the timing of the onset of flagellar assembly. FimV is necessary to prevent premature recruitment of early flagellar proteins, as shown by the early recruitment of all three flagellar proteins **(Fig. 5B and F and Fig. S7)**, and midcell accumulation of FlhF and FliF in predivisional Δ*fimV* cells **(Fig S8)**. Deletion of *flhF* does not reproduce this phenotype in any form, and therefore it is unlikely that the influence of FimV in the timing of flagellar protein recruitment is related to its role in the stabilization of FlhF interaction with the cell pole. We

are not aware of previous studies connecting FimV function to the timing of flagellar assembly. The biological relevance of the correct timing in the initiation of flagellar is as of now unclear and will be a subject of further investigation in the near future.

While preparing this manuscript, we have become aware of a preprint (Arroyo-Pérez *et al*., 2024) that documents the involvement of FimV and the novel protein FipA in the recruitment of FlhF to the cell pole and the interplay of all three proteins in the recruitment of EBB components in *V. parahaemolyticus, P. putida, and S. putrefaciens*. While this manuscript is largely focused on the biochemical interactions between the proteins involved, we have observed a number of overlapping results that are in any case generally consistent with our own observations.

MATERIALS AND METHODS

Bacterial strains and growth conditions

Bacterial strains used in this work are listed in **Table S1**. Liquid cultures of *E. coli* and *P. putida* were routinely grown in lysogeny broth (LB) (Sambrook & Russell, 2000) at 37 ºC and 30 ºC, respectively, with 180 rpm shaking. For solid media, American Bacteriological Agar (Condalab) was added to a final concentration of 15 g l^{-1}. When needed, antibiotics and other compounds were added at the following concentrations: ampicillin (100 mg l^{-1}), carbenicillin (500 mg l^{-1}), chloramphenicol (15 mg l^{-1}), rifampicin (20 mg l^{-1}), gentamycin (10 mg l^{-1}), kanamycin (25 mg l^{-1}), 3-methylbenzoate (3MB) (3 mM), 5-bromo-4-chloro-3-indoyl-β-D-galactopyranoside (X-gal) (25 mg l^{-1}) and sodium salicylate (2 mM). All reagents were purchased from Sigma-Aldrich.

Plasmid and strain construction

Plasmids and oligonucleotides used in this work are summarized in **Table S1.** All DNA manipulations were performed following standard protocols (Sambrook & Russell, 2000). Restriction and modification enzymes were used following to the manufacturer's instructions (New England Biolabs). PCR amplifications were carried out using Q5® High-Fidelity DNA Polymerase (New England Biolabs) for cloning and DreamTaq™ DNA Polymerase (Thermo Fisher) to verify plasmid constructions and chromosomal manipulations. One-step isothermal dsDNA Gibson assembly was performed as described (Gibson, 2011). *E. coli* DH5α was used as host strain for cloning procedures. Cloning steps involving PCR were verified by commercial Sanger sequencing (Stab Vida). Plasmid DNA was transferred to *E. coli* strains by transformation (Inoue *et al*., 1990), and to *P. putida* by triparental mating (Espinosa-Urgel *et al*., 2000) or electroporation (Choi *et al*., 2006). Site-specific integration of miniTn7-derivatives in *P. putida* strains was performed as previously described (Choi *et al*., 2005), and PCR-verified. Specific details of plasmid and strain construction are provided as **Supplementary Materials and Methods**.

Swimming motility assays

Swimming assays were adapted from Parkinson (1976). Fresh colonies were toothpick-inoculated in Tryptone-agar plates (1 % Bacto™ Tryptone [Difco], 0.5 % NaCl, 0.3 % Bacto™ Agar), and incubated at 30 ºC for 12 h. Digital images were taken and swimming halos diameter were measured using GIMP v2.10.12 (https://www.gimp.org) and normalized to the wild-type. At least, three biological replicates were assayed for each strain.

RNA extraction and RT-PCR

Total RNA from exponential phase cultures was isolated as described (García-González *et al*., 2005). Reverse transcription (RT) of 2 µg of total RNA into cDNA was carried out using the High-Capacity cDNA Reverse Transcription kit (Applied Biosystems) following the manufacturer's instructions. Amplification reactions were performed using 50 ng of cDNA as template in a 30-cycle PCR program, using appropriate oligonucleotides and Illustra™ PuReTaq™ Ready-To-Go™ PCR Beads (GE Healthcare). Positive and negative controls were performed with 50 ng of genomic DNA or 500 ng of total RNA as templates, respectively. The obtained RT-PCR products were resolved by 1 % agarose gel electrophoresis and visualized by ethidium bromide staining.

***In vivo* gene expression assays**

For end-point fluorescence assays of strains harboring *gfp-lacZ* transcriptional fusions to different promoters, overnight LB cultures supplemented with the corresponding antibiotics were diluted in 3 mL of the same medium to an A_{600} of 0.01 and incubated at 30 ºC with 180 rpm shaking until reaching A_{600} of 0.4-0.6 (exponential phase). Samples of 1 mL were withdrawn and cells were washed three times in phosphate-buffered saline (PBS). Cells were resuspended in 500 µL of PBS and 150 µL were dispensed by triplicate into the wells of Costar® 96-well polystyrene plates (Corning). A_{600} and GFP fluorescence (485 nm excitation, 535 nm emission, gain value set to 55) were measured in a Tecan Spark 10M microplate reader.

For β-galactosidase assays, the strains bearing *gfp-lacZ* transcriptional fusions were grown and diluted as described above. Growth was stopped when reaching exponential phase, and β-galactosidase activity was determined from sodium dodecyl sulfate- and chloroform-permeabilized cells as previously described (Miller, 1993). At least three biological replicates were assayed for each strain.

Protein secretion assay

Overnight cultures of strains expressing FlgM-FLAG were 100-fold diluted in 50 mL of LB medium supplemented with 2 mM salicylate and grown to A_{600} of 4. Cells were harvested by centrifugation (5000 *g*, 4 ºC, 15 min) and culture supernatants were collected for further precipitation. To increase the detection threshold in the intracellular fraction, pelleted cells were resuspended in 5 mL of cold buffer B (20 mM Tris-HCl pH 8.0, 150 mM NaCl, 0.5 % Nonidet P-40) and disrupted by sonication. Soluble fractions were rotating-incubated overnight at 4 ºC with 20 µL of buffer-equilibrated Anti-FLAG® M2 magnetic beads (Sigma-Aldrich), followed by 10 washes with 1 mL of the same buffer. Culture supernatants were filtered through Millipore membranes with 0.45 µM pore-size (Merck) and TCA was added to a final concentration of 10 % (v/v). After overnight incubation at 4 ºC, precipitates were collected by centrifugation (8000 *g*, 4 ºC, 30 min) and washed 3 times with 1 mL cold acetone. Protein pellets were dried for 10 min at 100 ºC. Precipitated supernatants and immunoprecipitated soluble cell fractions were further analyzed by Western-Blot.

SDS-PAGE and Western-Blot analysis

Protein samples were mixed with 2x loading buffer (150 mM Tris-HCl pH 6.8, 20 % glycerol, 4% SDS, 0.1 % bromophenol blue, 10 % β-mercaptoethanol) and boiled at 100 ºC for 10 min. Samples were centrifuged at 18000 *g* for 1 min and supernatants were separated on 12.5 % SDS-PAGE gels. Proteins were transferred to nitrocellulose membranes using a Trans-Blot Turbo Transfer System (Bio Rad). Membrane was blocked for 2 h at room temperature in blocking solution (3 % fat-free milk in TBS buffer with 1 % Tween 20). Blocked

membrane was incubated overnight at 4 ºC with primary antibody anti-FLAG (F3165, Sigma-Aldrich, 1:2000 dilution), washed 3 times in TBS with 1% Tween 20 (TBS-T), probed for 2 h at 4 ºC with secondary antibody anti-mouse HRP-conjugated (31430, Thermo Fischer, 1:10000 dilution), and washed with TBS-T as before. Membranes were added Pierce™ ECL Western Blotting Substrate (Thermo Fischer) and chemiluminescent signal was revealed using a ChemiDoc MP instrument (Bio-Rad) with a exposure time of 800 s. Image Lab software (Bio-Rad) was employed for image analysis.

Time-lapse fluorescence microscopy

Overnight cultures were 100-fold diluted in LB medium and grown to early-exponential phase (A_{600} of 0.2-0.3). Culture drops (2 µL) were placed on LB-agarose pads (1 % [w/v] agarose in 10 % [v/v] LB, to minimize background fluorescence) in glass slides and cells were imaged every 5 min using an Axio Imager.Z2 (Zeiss) microscope equipped with a Plan-Apochromat 63x/1.40 Oil Ph 3 M27 contrast objective lens and an ORCA-Flash 4.0 LT digital CMOS camera (Hamamatsu, pixel size: 0.1031 µm), controlled by the Zeiss ZEN 2 (Blue edition) software enabling software autofocus for focus maintenance over time. Phase contrast and GFPmut3 fluorescence images were respectively acquired using a TL Vis-LED Lamp (4.91 Volt, exposure time of 50 ms) and the LED module 470 nm from a Colibri.2 LED light source using a Zeiss 38 HE Green Fluorescent Prot. filter (excitation filter BP: 450/490 nm, emission filter BP: 500/550 nm, exposure time of 500 ms).

Confocal microscopy

Overnight cultures were 100-fold diluted in LB medium and grown to exponential phase (A_{600} of 0.4-0.6). Cells from 1 mL samples were harvested by centrifugation at 5000 *g* for 5 min and washed three times in PBS to remove LB. Flagellar filaments of strains expressing $FliC^{S267C}$ were stained by gently resuspending cells in 50 µL of PBS containing 5 µg/mL Alexa Fluor™ 488 C_5 maleimide (Molecular Probes), followed by incubation for 5 min at room temperature in the dark (Hintsche *et al*., 2017). Cells were washed three times for

excess dye removal. For membrane staining, cells were resuspended in 100 µL of PBS containing 5 µg/mL FM™ 4-64 (Molecular Probes). After incubation for 5 min at room temperature in the dark, 2 µL drops were immediately placed on 1 % agarose pads made with deionized water to be imaged using an Axio Observer7 confocal microscope (Zeiss) equipped with a CSU-W1 spinning disk module (Yokogawa). Images were taken using a Zeiss α Plan-Apochromat 100x/1.46 Oil DIC M27 objective lens and a Prime 95B CMOS camera (Teledyne Photometrics, pixel size: 0.1099 µm), controlled by the SlideBook 6 software. GFPmut3 and Alexa Fluor™ 488-labeled $FliC^{S267C}$ fluorescence was excited with the 488 nm laser line and collected with emission filter 525/50 nm, while FM™ 4-64 was excited at 561 nm and collected with a 617/73 filter (exposure time of 1000 ms). Exposure times for GFPmut3-tagged FimV, FlhF, FliF and FliM were 300 ms, and 100 ms for Alexa Fluor™ 488-labeled $FliC^{S267C}$. For each image, 7 Z-sections were collected with a step size of 0.33 µm.

Microscopy image analysis

Microscopy images processing and analysis were performed using Fiji software v1.53t (Schneider *et al*., 2012). Background subtraction of the fluorescence signal from GFPmut3, Alexa Fluor™ 488 C_5 maleimide and FM™ 4-64 was set to a rolling ball radius of 20 pixels. In time-lapse fluorescence images, stacks were aligned using plugin StackReg (Thévenaz *et al*., 1998). Confocal images are shown as maxima projections of 7 Z- sections of the 525/50 channel, merged with the 617/73 channel showing the focal plane with the cell contour. Cell segmentation, maxima and foci detection, and cell measurements from confocal images were performed using MicrobeJ v5.13I plugin (Ducret *et al*., 2016). Unless otherwise stated, default parameters were applied. Cell perimeter detection was performed on the lowest Z-plane of the brightfield channel using the rod-shaped descriptor (area: 1-9 μm^2, length: 2-5.5 µm, width: 0.5-3 µm). The old cell pole was defined as the one showing the highest maxima intensity from the 525/50 channel. Images of three independent assays

showing the same fluorescence-labeled protein were batched-processed using the same maxima/foci tolerance and Z-score parameters, with a minimal intensity cutoff value of 200 and foci area of 0.02-max μm^2. A Gaussian-fitting algorithm was applied to discriminate between two close foci (radius: 1 pixel, method: oval, iterations: 1000, minimal r^2 for optimization: 0.9). A tolerance distance of 0.3 µm outside the segmented cell boundary was set for maxima/foci association to parent cells. Analyzed images were manually inspected to confirm that the majority of cells were properly assigned. Shape descriptors, medial axis profiles, polarity, maxima/foci intensities and parent localization associations were recorded for each strain. Demographic representations of the fluorescence intensity of the 525/50 channel of the medial profile (represented as the mean orthogonal projection of the fluorescence values along the medial axis) were performed for 500 randomized cells of each strain, sorted by cell length. MicrobeJ analysis-derived data were collected from three independent sets of 500 randomized cells within datasets containing at least 2000 segmented cells for each strain. Alexa Fluor™ 488-labeled $FliC^{S267C}$ filaments were manually inspected in 500 randomized cells from sets of 8 images containing 100-200 segmented cells for each strain.

Statistical analysis

Statistical treatment of the data was performed using GraphPad Prism v8.3.0 software. Results are reported as the average and standard deviation of at least three biological replicates or image datasets, or median and 95% confidence interval for the median for fluorescence foci quantification. Significance of the differences among strains was evaluated by means of the two-tailed Student's t-test for unpaired samples not assuming equal variance.

Bioinformatics analyses

Similarity between FimV/HubP proteins was scored using BLASTP at the National Center for Biotechnology Information web site (https://blast.ncbi.nlm.nih.gov/Blast.cgi) (Altschul *et al*., 1990).

ACKNOWLEDGMENTS

We wish to thank Enrique Flores, Antonia Herrero, Carmen Beuzón and Javier Ruiz-Albert for thoughtful advice and discussion. This work was funded by grants PGC2018-097151-B-100 and PID2021-126121-NB-I00 of the Spanish Ministerio de Ciencia e Innovación, by a predoctoral Formación de profesorado Universitario contract 19/02899 of the Spanish Ministerio de Educación y Formación Profesional, awarded to M P-S, and by an EMBO Scientific Exchange Grant 9458 from the European Molecular Biology Organization, awarded to M P-S to visit FC's laboratory.

REFERENCES

1. Altegoer F, Schuhmacher J, Pausch P, Bange G. From molecular evolution to biobricks and synthetic modules: a lesson by the bacterial flagellum. 2014. Biotechnol Genet Eng Rev 30(1-2):49-64.
2. Chevance FF, Hughes KT. Coordinating assembly of a bacterial macromolecular machine. 2008. Nat Rev Microbiol 6(6):455-65.
3. Terashima H, Kojima S, Homma M. Flagellar motility in bacteria structure and function of flagellar motor. 2008. Int Rev Cell Mol Biol 270:39-85.
4. Matilla MA, Krell T. Chemoreceptor-based signal sensing. 2017. Curr Opin Biotechnol 45:8-14.
5. Smith TG, Hoover TR. Deciphering bacterial flagellar gene regulatory networks in the genomic era. 2009. Adv Appl Microbiol 67:257-95.
6. Macnab RM. Flagella and motility. In: Neidhardt F C, Curtiss III R, Ingraham JL, Lin ECC, Low KB, Magasanik B, Reznikoff W S, Riley M, Schaechter M, Umbarger HE, editors. *Escherichia coli* and *Salmonella*: cellular and molecular biology. 2nd ed. 1996. Washington, D.C: ASM Press pp. 123–145
7. Martínez-García E, Nikel PI, Chavarría M, de Lorenzo V. The metabolic cost of flagellar motion in *Pseudomonas putida* KT2440. 2014. Environ Microbiol 16(1):291-303.
8. Leifson E. Staining, shape and arrangement of bacterial flagella. 1951. J Bacteriol 62(4):377-89.
9. Schuhmacher JS, Thormann KM, Bange G. How bacteria maintain location and number of flagella? 2015. FEMS Microbiol Rev 39(6):812-22.
10. Amako K, Umeda A. Flagellation of *Pseudomonas aeruginosa* during the cell division cycle. 1982. Microbiol Immunol 26(2):113-7.

11. Martins Dos Santos VA, Heim S, Moore ER, Strätz M, Timmis KN. Insights into the genomic basis of niche specificity of *Pseudomonas putida* KT2440. 2004. Environ Microbiol 6(12):1264-86.

12. Leal-Morales A, Pulido-Sánchez M, López-Sánchez A, Govantes F. Transcriptional organization and regulation of the *Pseudomonas putida* flagellar system. 2022. Environ Microbiol 24(1):137-157.

13. Rodríguez-Herva JJ, Duque E, Molina-Henares MA, Navarro-Avilés G, Van Dillewijn P, De La Torre J, Molina-Henares AJ, La Campa AS, Ran FA, Segura A, Shingler V, Ramos JL. Physiological and transcriptomic characterization of a *fliA* mutant of *Pseudomonas putida* KT2440. 2010. Environ Microbiol Rep 2(3):373-80.

14. Kazmierczak BI, Hendrixson DR. Spatial and numerical regulation of flagellar biosynthesis in polarly flagellated bacteria. 2013. Mol Microbiol 88(4):655-63.

15. Navarrete B, Leal-Morales A, Serrano-Ron L, Sarrió M, Jiménez-Fernández A, Jiménez-Díaz L, López-Sánchez A, Govantes F. Transcriptional organization, regulation and functional analysis of *flhF* and *fleN* in *Pseudomonas putida*. 2019. PLoS One 14(3):e0214166.

16. Carter T, Buensuceso RN, Tammam S, Lamers RP, Harvey H, Howell PL, Burrows LL. The type IVa pilus machinery is recruited to sites of future cell division. 2017. mBio 8(1):e02103-16.

17. Bense S, Bruchmann S, Steffen A, Stradal TEB, Häussler S, Düvel J. Spatiotemporal control of FlgZ activity impacts *Pseudomonas aeruginosa* flagellar motility. 2019. Mol Microbiol 111(6):1544-1557.

18. Schniederberend M, Williams JF, Shine E, Shen C, Jain R, Emonet T, Kazmierczak BI. Modulation of flagellar rotation in surface-attached bacteria: A pathway for rapid surface-sensing after flagellar attachment. 2019. PLoS Pathog 15(11):e1008149.

19. Nicastro GG, Kaihami GH, Pulschen AA, Hernandez-Montelongo J, Boechat AL, de Oliveira Pereira T, Rosa CGT, Stefanello E, Colepicolo P, Bordi C, Baldini RL. c-di-GMP-related phenotypes are modulated by the interaction between a diguanylate cyclase and a polar hub protein. 2020. Sci Rep 10(1):3077.

20. Buensuceso RN, Nguyen Y, Zhang K, Daniel-Ivad M, Sugiman-Marangos SN, Fleetwood AD, Zhulin IB, Junop MS, Howell PL, Burrows LL. The conserved tetratricopeptide repeat-containing C-terminal domain of *Pseudomonas aeruginosa* FimV is required for its cyclic AMP-dependent and -independent functions. 2016. J Bacteriol 198(16):2263-74.

21. Wehbi H, Portillo E, Harvey H, Shimkoff AE, Scheurwater EM, Howell PL, Burrows LL. The peptidoglycan-binding protein FimV promotes assembly of the *Pseudomonas aeruginosa* type IV pilus secretin. 2011. J Bacteriol 193(2):540-50.

22. Buensuceso RNC, Daniel-Ivad M, Kilmury SLN, Leighton TL, Harvey H, Howell PL, Burrows LL. Cyclic AMP-independent control of twitching motility in *Pseudomonas aeruginosa*. 2017. J Bacteriol 199(16):e00188-17.

23. Yamaichi Y, Bruckner R, Ringgaard S, Möll A, Cameron DE, Briegel A, Jensen GJ, Davis BM, Waldor MK. A multidomain hub anchors the chromosome segregation and chemotactic machinery to the bacterial pole. 2012. Genes Dev 26(20):2348-60.

24. Rossmann F, Brenzinger S, Knauer C, Dörrich AK, Bubendorfer S, Ruppert U, Bange G, Thormann KM. The role of FlhF and HubP as polar landmark proteins in *Shewanella putrefaciens* CN-32. 2015. Mol Microbiol 98(4):727-42.

25. Takekawa N, Kwon S, Nishioka N, Kojima S, Homma M. HubP, a polar landmark protein, regulates flagellar number by assisting in the proper polar localization of FlhG in *Vibrio alginolyticus*. 2016. J Bacteriol 198(22):3091-3098.

26. Arroyo-Pérez EE, Ringgaard S. Interdependent polar localization of FlhF and FlhG and their importance for flagellum formation of *Vibrio parahaemolyticus*. 2021. Front Microbiol 12:655239.

27. Altinoglu I, Abriat G, Carreaux A, Torres-Sánchez L, Poidevin M, Krasteva PV, Yamaichi Y. Analysis of HubP-dependent cell pole protein targeting in *Vibrio cholerae* uncovers novel motility regulators. 2022. PLoS Genet 18(1):e1009991. Erratum in: 2022. PLoS Genet 18(3):e1010094.

28. Rick T, Kreiling V, Höing A, Fiedler S, Glatter T, Steinchen W, Hochberg G, Bähre H, Seifert R, Bange G, Knauer SK, Graumann PL, Thormann KM. GGDEF domain as spatial on-switch for a phosphodiesterase by interaction with landmark protein HubP. 2022. NPJ Biofilms Microbiomes 8(1):35.

29. Kubori T, Yamaguchi S, Aizawa S. Assembly of the switch complex onto the MS ring complex of *Salmonella typhimurium* does not require any other flagellar proteins. 1997. J Bacteriol 179(3):813-7.

30. Boll JM, Hendrixson DR. A regulatory checkpoint during flagellar biogenesis in *Campylobacter jejuni* initiates signal transduction to activate transcription of flagellar genes. 2013 mBio 4(5):e00432-13.

31. Morimoto YV, Ito M, Hiraoka KD, Che YS, Bai F, Kami-ike N, Namba K, Minamino T. Assembly and stoichiometry of FliF and FlhF in *Salmonella* flagellar basal body. 2014. Mol Microbiol 91(6):1214-26.

32. Li H, Sourjik V. Assembly and stability of flagellar motor in *Escherichia coli*. 2011. Mol Microbiol 80(4):886-99.

33. Vischer NO, Verheul J, Postma M, van den Berg van Saparoea B, Galli E, Natale P, Gerdes K, Luirink J, Vollmer W, Vicente M, den Blaauwen T. Cell age dependent concentration of *Escherichia coli* divisome proteins analyzed with ImageJ and ObjectJ. 2015. Front Microbiol 6:586.

34. Macnab RM. How bacteria assemble flagella. 2003. Annu Rev Microbiol 57:77-100.

35. Apel D, Surette MG. Bringing order to a complex molecular machine: the assembly of the bacterial flagella. 2008. Biochim Biophys Acta 1778(9):1851-8.

36. Armitage JP, Berry RM. Assembly and dynamics of the bacterial flagellum. 2020. Annu Rev Microbiol 74:181-200.

37. Pandza S, Baetens M, Park CH, Au T, Keyhan M, Matin A. The G-protein FlhF has a role in polar flagellar placement and general stress response induction in *Pseudomonas putida*. 2000. Mol Microbiol 36(2):414-23.

38. Inclan YF, Persat A, Greninger A, Von Dollen J, Johnson J, Krogan N, Gitai Z, Engel JN. A scaffold protein connects type IV pili with the Chp chemosensory system to mediate activation of virulence signaling in *Pseudomonas aeruginosa*. 2016. Mol Microbiol 101(4):590-605.

39. Park S, Yoon J, Lee CR, Lee JY, Kim YR, Jang KS, Lee KH, Seok YJ. Polar landmark protein HubP recruits flagella assembly protein FapA under glucose limitation in *Vibrio vulnificus*. 2019. Mol Microbiol 112(1):266-279.

40. Dornes A, Schmidt LM, Mais CN, Hook JC, Pané-Farré J, Kressler D, Thormann K, Bange G. Polar confinement of a macromolecular machine by an SRP-type GTPase. 2024. Nat Commun 15(1):5797.

41. Galli E, Paly E, Barre FX. Late assembly of the *Vibrio cholerae* cell division machinery postpones septation to the last 10% of the cell cycle. 2017. Sci Rep 7:44505.

42. Kusumoto A, Shinohara A, Terashima H, Kojima S, Yakushi T, Homma M. Collaboration of FlhF and FlhG to regulate polar-flagella number and localization in *Vibrio alginolyticus*. 2008. Microbiology (Reading) 154(Pt 5):1390-1399.

43. Green JC, Kahramanoglou C, Rahman A, Pender AM, Charbonnel N, Fraser GM. Recruitment of the earliest component of the bacterial flagellum to the old cell division

pole by a membrane-associated signal recognition particle family GTP-binding protein. 2009. J Mol Biol 391(4):679-90.

44. Ainsaar K, Tamman H, Kasvandik S, Tenson T, Hõrak R. The $TonB_m$-PocAB system Is required for maintenance of membrane integrity and polar position of flagella in *Pseudomonas putida*. 2019. J Bacteriol 201(17):e00303-19.

45. Katayama E, Shiraishi T, Oosawa K, Baba N, Aizawa S. Geometry of the flagellar motor in the cytoplasmic membrane of *Salmonella typhimurium* as determined by stereo-photogrammetry of quick-freeze deep-etch replica images. 1996. J Mol Biol 255(3):458-75.

46. Kubori T, Yamaguchi S, Aizawa S. Assembly of the switch complex onto the MS ring complex of *Salmonella typhimurium* does not require any other flagellar proteins. 1997. J Bacteriol 179(3):813-7.

47. Murray TS, Kazmierczak BI. FlhF is required for swimming and swarming in *Pseudomonas aeruginosa*. 2006. J Bacteriol 188(19):6995-7004.

48. Correa NE, Peng F, Klose KE. Roles of the regulatory proteins FlhF and FlhG in the *Vibrio cholerae* flagellar transcription hierarchy. 2005. J Bacteriol 187(18):6324-32.

49. Kim SM, Lee DH, Choi SH. Evidence that the *Vibrio vulnificus* flagellar regulator FlhF is regulated by a quorum sensing master regulator SmcR. 2012. Microbiology (Reading) 158(Pt 8):2017-2025.

50. Ren F, Lei T, Song Z, Yu T, Li Q, Huang J, Jiao XA. Could FlhF be a key element that controls *Campylobacter jejuni* flagella biosynthesis in the initial assembly stage? 2018. Microbiol Res 207:240-248.

51. Li X, Chai Q, Zheng L, Huang P, Gundogdu O, Jiao X, Tang Y, Huang J. Investigating the role of BN-domains of FlhF involved in flagellar synthesis in *Campylobacter jejuni*. 2022. Microbiol Res 256:126944.

52. Niehus E, Gressmann H, Ye F, Schlapbach R, Dehio M, Dehio C, Stack A, Meyer TF, Suerbaum S, Josenhans C. Genome-wide analysis of transcriptional hierarchy and feedback regulation in the flagellar system of *Helicobacter pylori*. 2004. Mol Microbiol 52(4):947-61.

53. Arroyo-Pérez EE, Hook JC, Alvarado A, Wimmi S, Glatter T, Thormann KM, Ringgaard S. A conserved cell-pole determinant organizes proper polar flagellum formation. 2024. eLife 13:RP93004

54. Sambrook JE, Russell DW. Molecular Cloning, a Laboratory Manual. 2000. Cold Spring Harbor, New York, USA: Cold Spring Harbor Laboratory Press

55. Gibson DG. Enzymatic assembly of overlapping DNA fragments. 2011. Methods Enzymol. 2011;498:349-61.

56. Inoue H, Nojima H, Okayama H. High efficiency transformation of *Escherichia coli* with plasmids. 1990. Gene 96(1):23-8.

57. Espinosa-Urgel M, Salido A, Ramos J-L. Genetic analysis of functions involved in adhesion of *Pseudomonas putida* to seeds. 2000. J Bacteriol 182: 2363–2369.

58. Choi KH, Kumar A, Schweizer HP. A 10-min method for preparation of highly electrocompetent *Pseudomonas aeruginosa* cells: application for DNA fragment transfer between chromosomes and plasmid transformation. 2006. J Microbiol Methods 64(3):391-7.

59. Choi KH, Gaynor JB, White KG, Lopez C, Bosio CM, Karkhoff-Schweizer RR, Schweizer HP. A Tn7-based broad-range bacterial cloning and expression system. 2005. Nat Methods 2(6):443-8.

60. Parkinson JS. *cheA*, *cheB*, and *cheC* genes of *Escherichia coli* and their role in chemotaxis. 1976. J Bacteriol 126(2):758-70.

61. García-González V, Govantes F, Porrúa O, Santero E. Regulation of the *Pseudomonas* sp. strain ADP cyanuric acid degradation operon. 2005. J Bacteriol 187(1):155-67.

62. Miller JH. A short course in bacterial genetics – A laboratory manual and handbook for *Escherichia coli* and related bacteria. 1993. Cold Spring Harbor, New York: Cold Spring Harbor Laboratory Press.

63. Hintsche M, Waljor V, Großmann R, Kühn MJ, Thormann KM, Peruani F, Beta C. A polar bundle of flagella can drive bacterial swimming by pushing, pulling, or coiling around the cell body. 2017. Sci Rep 7(1):16771.

64. Schneider CA, Rasband WS, Eliceiri KW. NIH Image to ImageJ: 25 years of image analysis. 2012. Nat Methods 9(7):671-5.

65. Thévenaz P, Ruttimann UE, Unser M. A pyramid approach to subpixel registration based on intensity. 1998. IEEE Trans Image Process 7(1):27-41.

66. Ducret A, Quardokus EM, Brun YV. MicrobeJ, a tool for high throughput bacterial cell detection and quantitative analysis. 2016. Nat Microbiol 20;1(7):16077.

67. Altschul SF, Gish W, Miller W, Myers EW, Lipman DJ. Basic local alignment search tool. 1990. J Mol Biol 215(3):403-10.

FIGURES

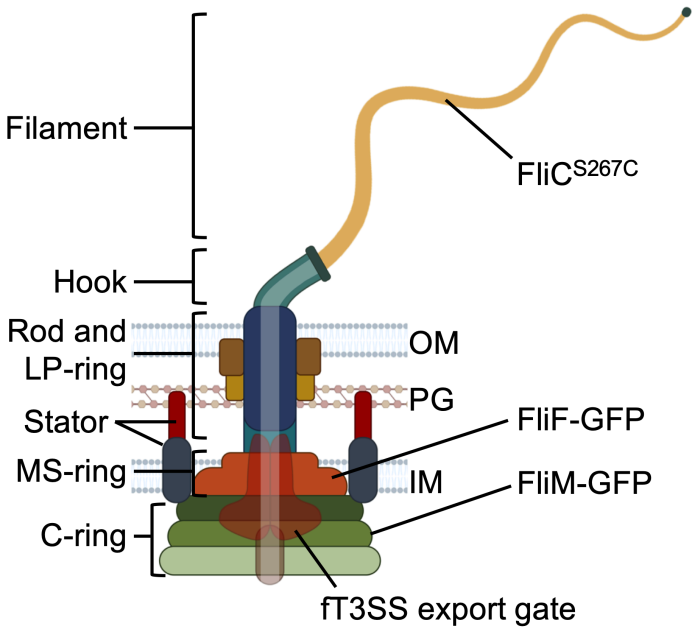

Figure 1. Structure of the Gram-negative flagellum. Cartoon depicting the archetypical structural units of the flagellum in Gram-negative bacteria and the location of the fluorescent flagellar protein derivatives used in this work: FliF-GFP (MS-ring), FliM-GFP (C-ring) and FliC^{S267C} (filament). OM: outer membrane; PG: peptidoglycan; IM: inner membrane; fT3SS: flagellar type III secretion system. Not drawn to scale. Created in part with Biorender.com.

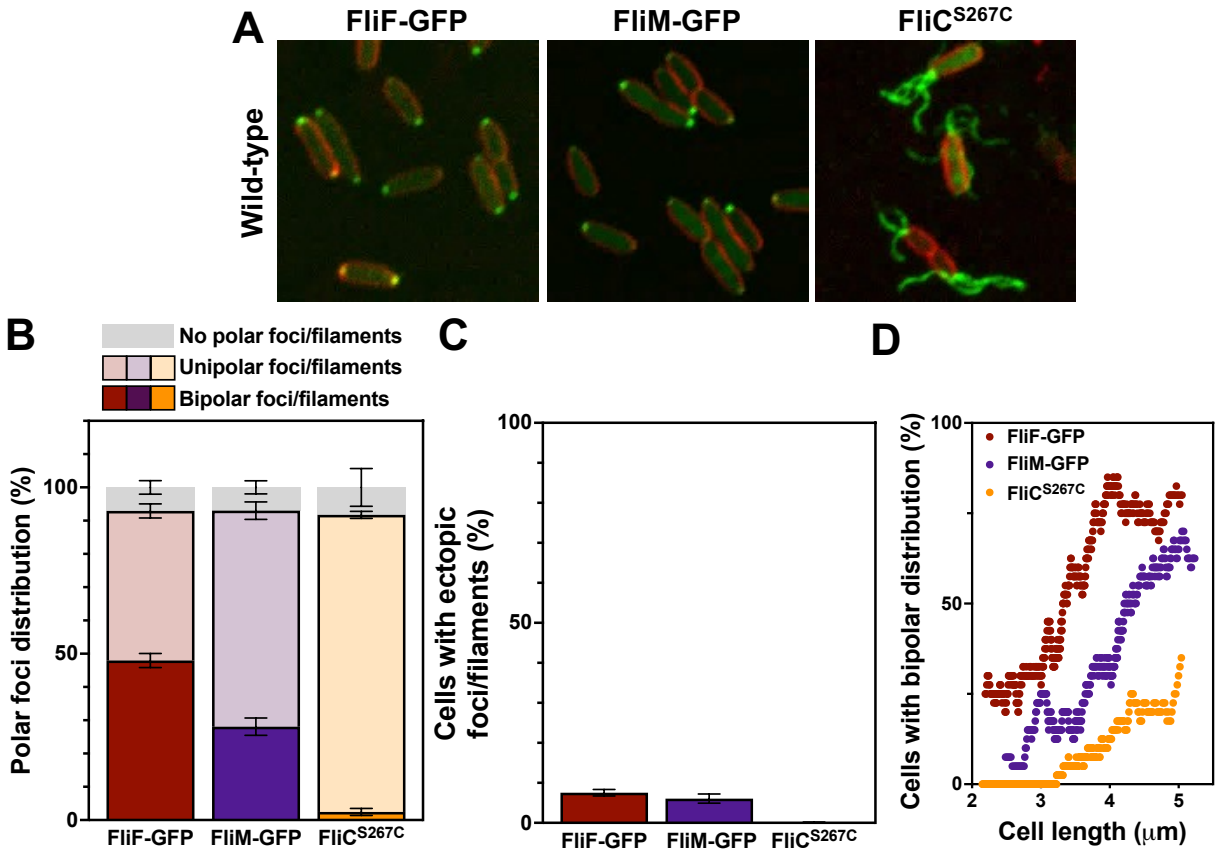

Figure 2. Polar localization of the flagellar structural proteins. A. Confocal microscopy images of wild-type cells expressing P*fliE-fliF-gfp*, P*fliL-fliM-gfp* or P*fliC-fliC*^{S267C} (green). Alexa Fluor™ 488 C5 maleimide was used for FliC^{S267C} filaments staining. FM™ 4-64 was used as membrane stain (red). Images are shown as the maxima projections of seven Z-sections of the green channel, merged with the red channel showing the cell contour at the focal plane. **B.** Frequency of wild-type cells bearing bipolar, unipolar or no polar FliF-GFP, FliM-GFP foci or FliC^{S267C} filaments. **C.** Frequency of wild-type cells bearing ectopic FliF-GFP, FliM-GFP foci or FliC^{S267C} filaments. **D.** Frequency of wild-type cells displaying bipolar distribution of FliF-GFP, FliM-GFP foci or FliC^{S267C} filaments *vs.* cell length (n=500 cells). Columns and error bars represent average and standard deviation of at least three separate replicates.

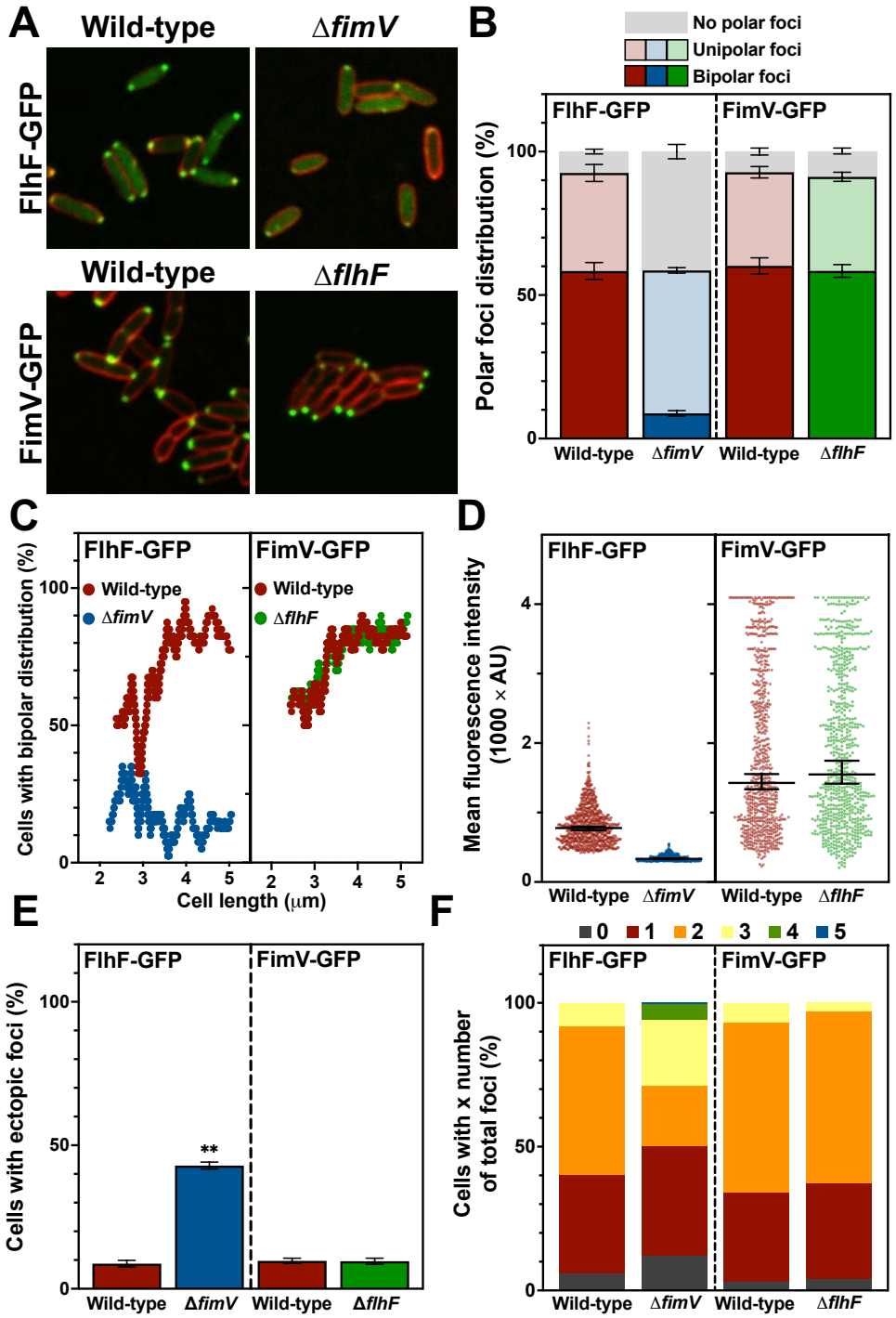

Figure 3. Intracellular location of FlhF and FimV. A. Confocal microscopy images of wild-type, Δ*fimV* and Δ*flhF* cells expressing P*flhF-flhF-gfp* or P*asd-fimV-gfp* (green). FM™ 4-64 was used as membrane stain (red). Images are shown as the maxima projections of seven Z-sections of the green channel, merged with the red channel showing the cell contour at the focal plane. **B.** Frequency of wild-type, Δ*fimV* or Δ*flhF* cells bearing bipolar, unipolar or no polar FlhF-GFP or FimV-GFP foci. **C.** Frequency of wild-type, Δ*fimV* or Δ*flhF* cells displaying bipolar distribution of FlhF-GFP or FimV-GFP foci *vs.* cell length (n=500 cells). **D.** Mean fluorescence intensity of polar FlhF-GFP or FimV-GFP foci in wild-type, Δ*fimV* or Δ*flhF* cells (n=500 cells). **E.** Frequency of wild-type, Δ*fimV* or Δ*flhF* cells bearing ectopic FlhF-GFP or FimV-GFP foci. **F.** Percentage of wild-type, Δ*fimV* or Δ*flhF* cells bearing 0, 1, 2, 3, 4 or 5 total FlhF-GFP or FimV-GFP foci. Columns and error bars represent average and standard deviation of at least three separate replicates. Points correspond to individual fluorescence intensity values, bars denote the median and the 95% confidence interval for the median (**D**). Stars denote *p*-values of the two-tailed Student's T test not assuming equal variance (*=p<0.05; **= p<0.01; ***= p<0.001; ****= p<0.0001).

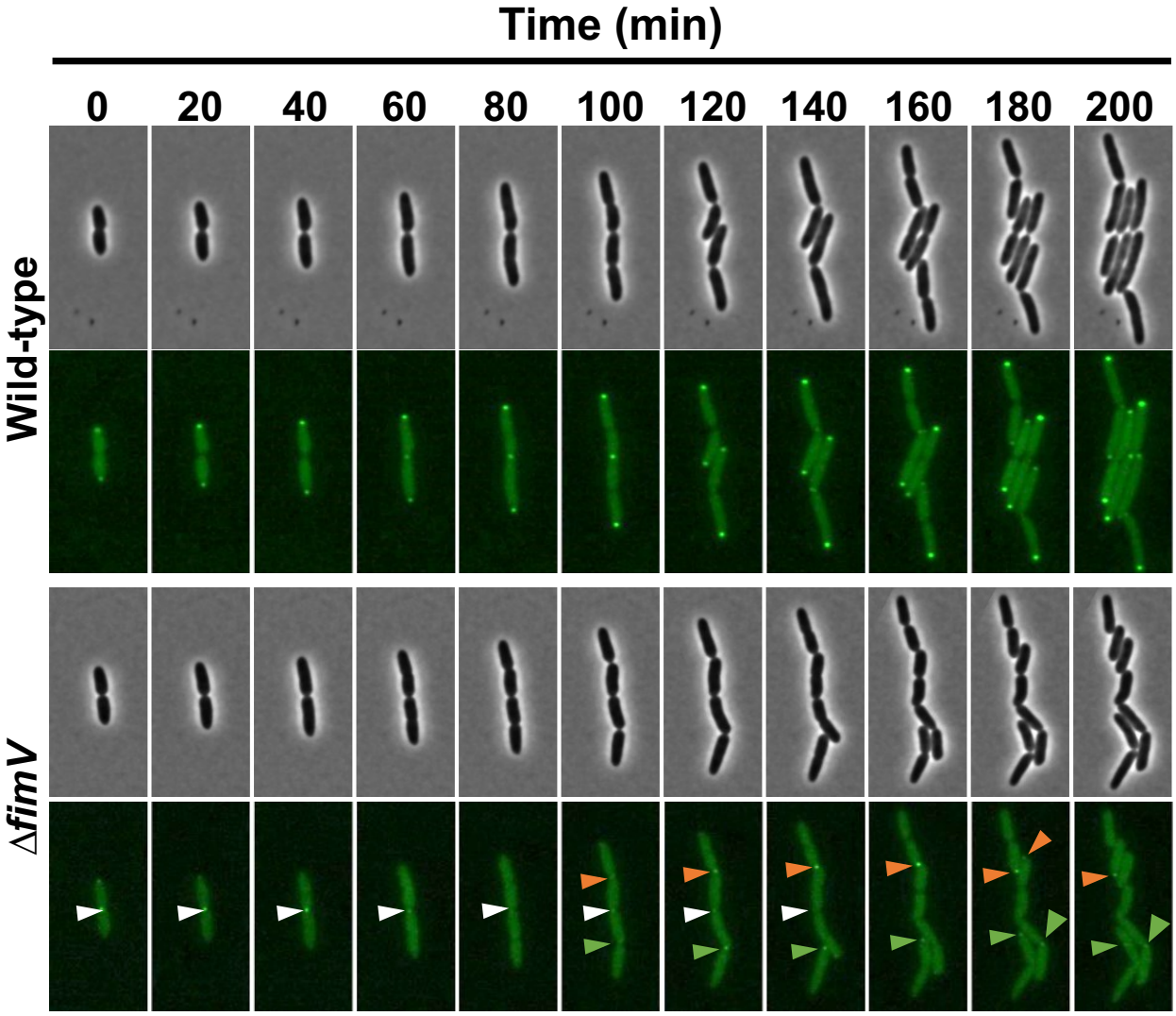

Figure 4. Accumulation dynamics of FlhF-GFP in the Δ*fimV* mutant. Time-lapse fluorescence microscopy images of wild-type and Δ*fimV* cells expressing P*flhF-flhF-gfp*. Phase contrast (first and third rows) and fluorescence (second and fourth rows) images are shown. Arrowheads indicate the evolution of three individual fluorescence foci over time.

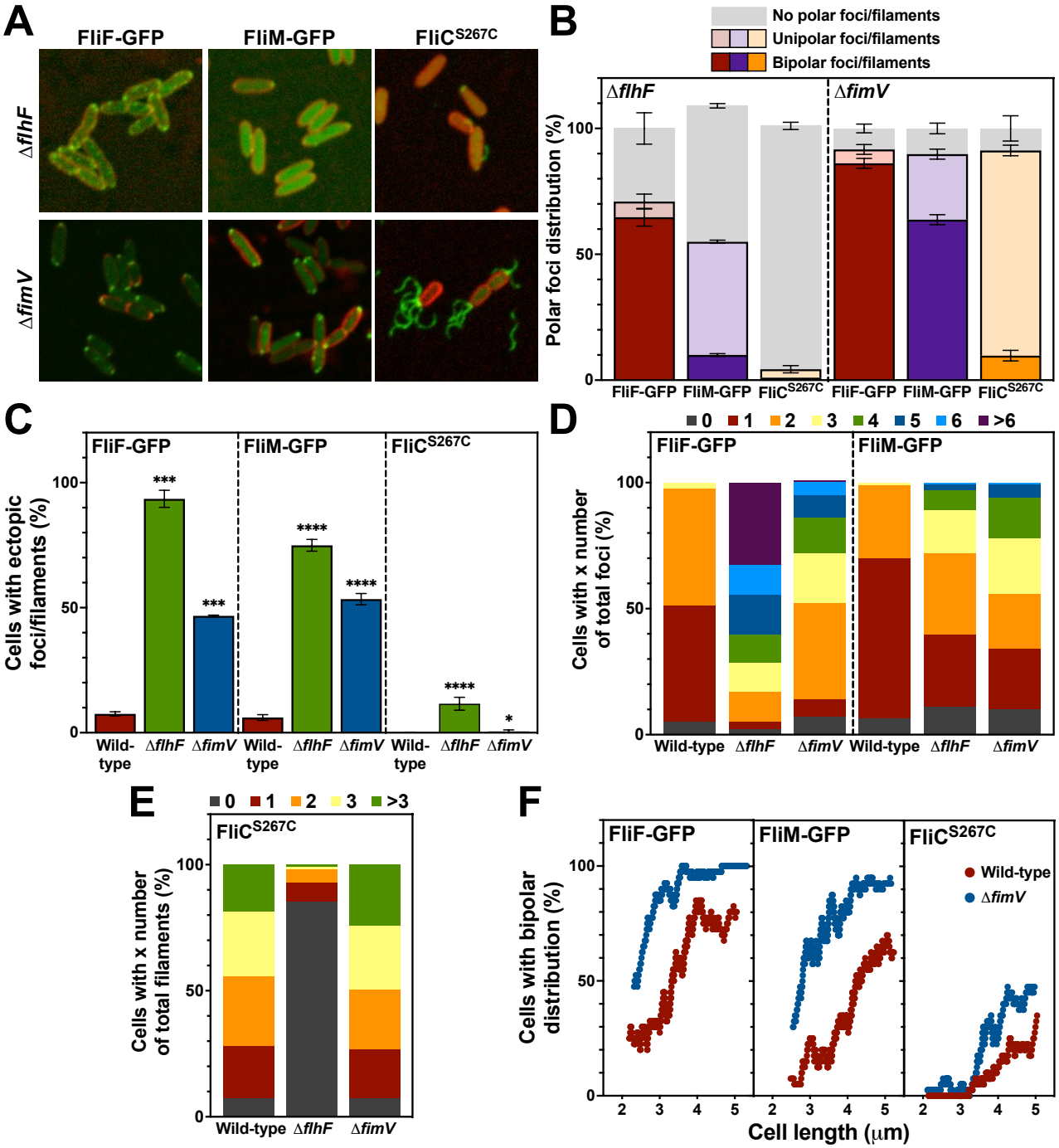

Figure 5. Cellular location of the flagellar structural proteins. A. Confocal microscopy images of Δ*fimV* and Δ*flhF* cells expressing P*fliE-fliF-gfp,* P*fliL-fliM-gfp* or P*fliC-fliC*^{S267C} (green). Alexa Fluor™ 488 C5 maleimide was used for FliC^{S267C} filament staining. FM™ 4-64 was used as membrane stain (red). Images are shown as the maxima projections of seven Z-sections of the green channel, merged with the red channel showing the cell contour at the focal plane. **B.** Frequency of Δ*fimV* or Δ*flhF* cells bearing bipolar, unipolar or no polar FliF-GFP or FliM-GFP foci or FliC^{S267C} filaments. **C.** Frequency of wild-type, Δ*fimV* or Δ*flhF* cells bearing ectopic FliF-GFP or FliM-GFP foci or FliC^{S267C} filaments. **D and E.** Percentage of wild-type, Δ*fimV* or Δ*flhF* cells bearing 0, 1, 2, 3, 4, 5, 6 or more than six total FliF-GFP or FliM-GFP foci (**D**) or 0, 1, 2, 3 or more than three total FliC^{S267C} filaments (**E**). **F.** Frequency of wild-type and Δ*fimV* cells displaying bipolar distribution of FliF-GFP or FliM-GFP foci or FliC^{S267C} filaments *vs.* cell length (n=500 cells **F.** Percentage of wild-type, Δ*fimV* or Δ*flhF* cells bearing 0, 1, 2, 3, 4 or 5 total FlhF-GFP or FimV-GFP foci. Columns and error bars represent average and standard deviation of at least three separate replicates. Stars denote p-values of the two-tailed Student's T test not assuming equal variance (*=p<0.05; **= p<0.01; ***= p<0.001; ****= p<0.0001).

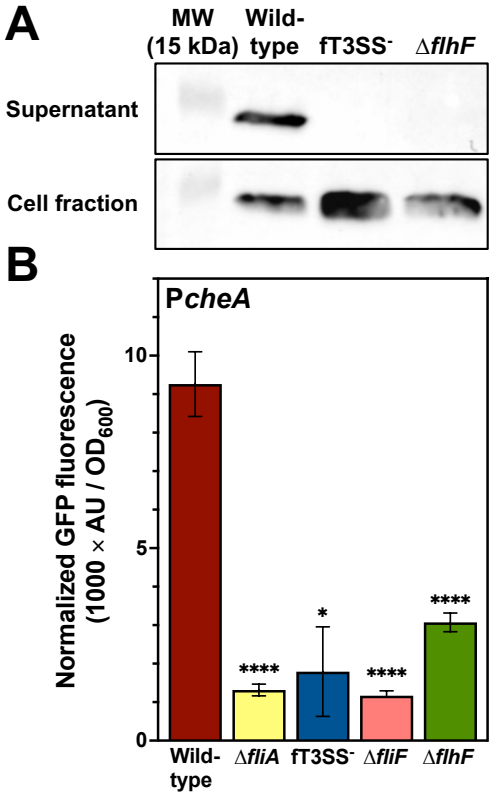

Figure 6. FlgM secretion and P*cheA* expression in the fT3SS$^-$ and Δ*flhF* mutants. A. Western blot analysis of FLAG-tagged FlgM in the culture supernatants (top) and cell fractions (bottom) of the wild-type, fT3SS$^-$ and Δ*flhF* strains. MW: molecular weight marker (15 kDa band shown). **B.** Normalized GFP fluorescence from exponential cultures of wild-type, Δ*fliA*, fT3SS$^-$, Δ*fliF* and Δ*flhF* strains bearing a transcriptional P*cheA-gfp* fusion. Columns and error bars represent average and standard deviation of at least three separate replicates. Stars denote p-values of the two-tailed Student's T test not assuming equal variance (*=p<0.05; **= p<0.01; ***= p<0.001; ****= p<0.0001).